Saf. Nucl. Waste Disposal, 3, 15–31, 2025
https://doi.org/10.5194/sand-3-15-2025

SaND
Safety of Nuclear Waste Disposal
Open Access

SAFENET-2 – fracture evolution in crystalline rocks (from lab to in situ scale)

Olaf Kolditz[1,7], Christopher McDermott[2], Jeoung Seok Yoon[3], Jörg Renner[4], Li Zhuang[5], Andrew Fraser-Harris[2], Michael Chandler[2], Samuel Graham[2], Ju Wang[6], and Mostafa Mollaali[1]

[1]Helmholtz Centre for Environmental Research UFZ, Department of Environmental Informatics, Leipzig, Germany
[2]School of Geosciences, The University of Edinburgh, Edinburgh, United Kingdom
[3]DynaFrax UG, Potsdam, Germany
[4]Institute for Geology, Mineralogy, and Geophysics, Ruhr-Universität Bochum, Bochum, Germany
[5]School of Resources and Safety Engineering, Chongqing University, Chongqing, China
[6]Beijing Research Institute of Uranium Geology BRIUG, Beijing, China
[7]Applied Environmental Systems Analysis, Technische Universität Dresden, Dresden, Germany

Correspondence: Olaf Kolditz (olaf.kolditz@ufz.de)

Received: 7 August 2024 – Discussion started: 6 September 2024
Revised: 19 December 2024 – Accepted: 23 January 2025 – Published: 18 March 2025

Abstract. The DECOVALEX Task SAFENET is dedicated to advancing the understanding of fracture nucleation and evolution processes in crystalline rocks, with applications in nuclear waste management and geothermal reservoir engineering. Further improvements to fracture mechanics models are required in two distinct areas. Firstly, there is a need to enhance numerical methods for fracture mechanics under varying thermo-hydro-mechanical (THM) conditions. Secondly, there is a requirement to develop applied tools for performance and safety assessment in the context of nuclear waste management, as well as for reservoir optimisation in geothermal applications. Building on the achievements of SAFENET, which concentrated on benchmarking fracture models and experimental laboratory analyses, SAFENET-2 is dedicated to extending and validating models from the laboratory to the field scale.

This paper gives a detailed description of the SAFENET-2 experimental programme work plan and modelling exercises. The experiments will be carried out at the rock mechanics laboratories of the University of Edinburgh and Chongqing University. For field data, the STIMTEC experiment at the Reiche Zeche teaching and research mine (Technische Universität Bergakademie Freiberg) is used. The individual steps of the Task are described in detail in this paper. As a result of SAFENET, the benchmark suite will be made available as interactive exercises via a web portal, thus promoting the concept of open science. The paper is a tool for teams to organise their work efficiently and is also an overview and insight for the community.

1 Introduction

DECOVALEX is a long-term international benchmarking project focusing on the systematic improvement of models for repository research. Multi-physical processes – so-called thermo-hydro-mechanico-chemical (THMC) processes, which can be used to describe the temporal and spatial evolution of repository systems in terms of continuum mechanics – play a special role (Birkholzer et al., 2024). DECOVALEX is an acronym for "Development of Coupled Models and their Validation against Experiments". The benchmarking philosophy has been continuously refined over numerous project phases. The basic building blocks, which have increasing complexity, are benchmarking exercises; experimental analysis; blind prediction; and, increasingly, performance assessments for repository systems. The development of reliable models is a major research chal-

lenge. It is essential for establishing acceptance in the broadest sense, i.e. both academic and social acceptance. (Flynn et al., 1992; Sjöberg, 2004; Sjöberg and Drottz-Sjöberg, 2008). In the context of benchmarking exercises, analytical solutions and/or code comparisons are employed for the purpose of academic, synthetic test examples. These are used to ascertain the accuracy of numerical models and/or to test the correct implementation of numerical methods. In the case of DECOVALEX Tasks, experiments from geotechnical and underground laboratories are selected on a systematic basis with a view toward validating the numerical models against measured data. The question of the transferability of the models from the laboratory to the in situ scale plays a central role in this process (experimental analysis). In this context, the term "validation" refers to the capacity of models to predict measurement outcomes that were not incorporated into the calibration process (blind prediction). In recent DECOVALEX projects, Tasks for the characterisation of parts of or complete repository systems in a geological context have also been defined and processed (performance assessment). The complete analysis of a repository system requires the handling of a significant computational burden. Consequently, the development of efficient computing methods, particularly parallel computing, is becoming a crucial aspect of DECOVALEX. Additionally, alternative approaches are being explored to identify suitable replacement models for the intricate coupled thermo-hydro-mechanical (THM) models utilising machine learning techniques (Bang et al., 2020; Hu et al., 2023; Hu and Pfingsten, 2023; Buchwald et al., 2024; Hu et al., 2024).

Notwithstanding the long history of DECOVALEX (Rutqvist et al., 2005; Chan et al., 2005), the SAFENET Task introduces fracture mechanics into the project for the first time in a comprehensive benchmarking exercise. SAFENET has a broader perspective; the abbreviation stands for "Safety Assessment of Fluid Flow, Shear, Thermal and Reaction Processes within Crystalline Rock Fracture Networks". To achieve SAFENET's first scientific goal of better understanding fracture initiation and evolution in crystalline rocks under hydro-mechanical and thermo-mechanical loading, a systematic experimental and modelling programme was organised and completed under Task G of DECOVALEX 2023 (experimental analyses). Three experimental programmes were carried out in Freiberg (Frühwirt et al., 2021), Seoul (Sun et al., 2021, 2023) and Edinburgh (McDermott et al., 2018; Fraser-Harris et al., 2020, 2025) to study mechanical and thermo-mechanical shear and stress-dependent permeability changes in fractured crystalline rocks.

Crystalline rocks are among the potential host rocks for nuclear waste repositories, particularly for the Nordic countries, Canada, Korea and Japan, which are rich in crystalline rock formations. A sound knowledge of the behaviour of crystalline rocks, particularly their strength as geological barriers, is of paramount importance. Therefore, the fracture mechanics of brittle rocks constitute the focus of SAFENET projects.

For numerical analyses, the modelling teams offer a wide range of continuum mechanics and discontinuous methods for the numerical modelling of fracture mechanics processes. Details of the numerical methods are described in Mollaali et al. (2023) and Bilke et al. (2019). The benchmarking exercises include plane and rough-fracture examples, as well as simple fracture networks. The main results of SAFENET-1 have recently been synthesised in Kolditz et al. (2025). SAFENET uses a systematic and experimental approach to numerically simulate mechanical (M), hydro-mechanical (HM) and thermo-mechanical (TM) fracture processes in brittle rocks. The Task team has introduced, applied and compared a wide range of numerical methods, including both continuum and discontinuum methods, for simulating related fracture processes (e.g. finite-element method (FEM), digital elevation model (DEM), cellular automata, numerical manifold method). Experimental data of SAFENET-1 are based on three key experiments, namely the Freiberg, GREAT cell and KICT experiments, which analyse M, HM and TM processes, respectively. Classic HM and THM benchmarking exercises serve as a common basis, using analytical solutions for a plane–line discontinuity in a poroelastic medium (Sneddon and Lowengrub, 1969) and a point heat source in a thermo-poroelastic medium (Booker and Savvidou, 1985; Chaudhry et al., 2019). These solutions also serve as a reference for rough fractures and simple fracture networks. An analysis of the constant-normal-load (CNL) experiment was carried out using microscopic and macroscopic approaches based on the Freiberg experiment. The GREAT cell experiments provided a database for evaluating the mechanical and hydro-mechanical responses of various rock samples (resin, greywacke, gneiss) in triaxial tests with a rotational stress field. Fracture permeability was determined as a function of normal stresses in the rotational stress field. The KICT experiments were used to investigate thermally induced shear slip and dilation processes.

SAFENET will also elaborate upon the potential of artificial intelligence (AI) concepts for benchmarking purposes with regard to the use of surrogate models for computational speed-up, quantification of uncertainties (Kurgyis et al., 2024), etc. AI methods are also gaining increasing attention in the field of nuclear waste management (BASE, 2023; Breitkreutz et al., 2023), particularly in the context of European initiatives such as EURAD (Claret et al., 2022; Prasianakis et al., 2020; Kolditz et al., 2023; Jacques et al., 2023; Kühn et al., 2012). However, the potential needs to be carefully assessed and exploited through concerted action.

2 SAFENET-2

2.1 Concept

Figure 1 illustrates the concept of the SAFENET-2 Task. Based on the findings presented in DECOVALEX 2023 regarding the examination of HM and TM processes, the subsequent phase of the investigation of fully coupled THM processes will focus on two distinct approaches, both commencing from HM (GREAT cell, McDermott et al., 2018; Fraser-Harris et al., 2020, 2025) and TM+H (thermoslip–flow cell) processes. In a series of previous works (Sun et al., 2021, 2023, 2024, 2025), the experimental basis for TM+H was developed. These approaches will encompass the analysis of temperature and hydraulic effects. The experimental programme has been designed with these objectives in mind. The GREAT cell is additionally equipped with a heating device. The thermoslip-flow cell allows heating, triaxial loading and additional fluid injection into a fractured specimen. The experimental setup is described in detail in Sect. 2.2.1 and 2.2.2. SAFENET-2 will focus on two areas: firstly, the improvement of numerical models based on laboratory experiments. The second area of focus is the transfer of knowledge from the laboratory to the field scale. The experimental basis at the field scale is provided by the STIMTEC experiment at the research mine Reiche Zeche, where stimulation tests with periodic pumping tests and high-resolution seismic monitoring have been conducted (Boese et al., 2021, 2022, 2023). In conjunction with the laboratory experimental data, the STIMTEC experiment will serve as a foundation for upscaling fracture models from the laboratory to the field scale with respect to hydromechanically induced fracture processes. The SAFENET-2 project incorporates a methodological phase. In this context, further development will be undertaken of numerical approaches to fracture mechanics, including those based on THM (e.g. phase field methods, discrete element methods). The potential of artificial intelligence (AI), including machine learning methods for the construction of surrogates for complex THM fracture mechanics models, will be investigated. Such surrogates may be trained from full-complexity THM models. Moreover, we will introduce novel benchmarking techniques that facilitate interactivity in collaborative endeavours through the utilisation of web-based Jupyter notebooks for online benchmarking.

The participating groups of SAFENET-2 are the Helmholtz Centre for Environmental Research (UFZ), Ruhr-Universität Bochum (RUB), the Federal Institute of Geosciences and Natural Resources (BGR), Technische Universität Bergakademie Freiberg (TUBAF), the Chinese Academy of Sciences (CAS), the Lawrence Berkeley National Laboratory (LBNL), the Sandia National Laboratory (SNL), the University of Edinburgh, DynaFrax, Chongqing University (CQU), the Korean Institute for Geosciences and Mineral Resources (KIGAM), and Taipower (TPC).

2.2 Experimental basis

The experimental basis of SAFENET-2 consists of laboratory experiments conducted at the University of Edinburgh in the UK (GREAT cell facility, Sect. 2.2.1) and at Chongqing University in China (Sect. 2.2.2). Experimental data from field experiments are derived from the teaching and research mine of Technische Universität Bergakademie Freiberg in Germany (Sect. 2.2.3).

2.2.1 GREAT cell large-lab-scale data

The GREAT cell facility at the University of Edinburgh (Fig. 2) provides the unique capability to create hydraulic fractures in rock samples under a controlled true-triaxial stress field ($\sigma_1 > \sigma_2 > \sigma_3$) and to change that stress field during the experiment, enabling the investigation of the impact of normal and shear stress on fracture permeability. The sample size is 200 mm diameter × 200 mm height, and strain is measured along the middle circumference of the cylinder. The strain is recorded using a fibre optic cable attached to the surface of the sample, allowing for a high spatial (every 2 mm) and temporal (100 Hz) resolution of the strain to be recorded and for the deformation during the process of fracturing to be recorded.

Two types of main experiments are available for the SAFENET-2 HM Task 2 (Fig. 1): (i) fracture creation and dynamic propagation experiments (three different loading conditions) and (ii) fracture circulation experiments.

(i) *Fracture initiation experiments.* Three 20 cm diameter cylindrical rock samples were manufactured from Freiberg gneiss. These samples were each used to conduct fluid injection experiments under three distinct stress states. For the Freiberg gneiss, an unconfined press was used to provide the axial load, and an unconfined hydraulic fracture was created using fluid pressure in a borehole. The Luna fibre optic strain gauges (https://lunainc.com/capability/strain, last access: 14 March 2025) and logging equipment were used to measure the dynamic circumferential strain during the fracturing process. A schematic of the sample and borehole with respect to the applied stresses is illustrated in Fig. 3a. The evolution of borehole fluid pressure during the fracturing of the Freiberg gneiss sample under uniaxial compressive strength is shown in Fig. 3b. The early part of this plot corresponds to the application of an 8 MPa axial load, during which time no increase in borehole fluid pressure was applied. Fracturing was achieved by flowing water at a constant rate of $Q_i = 1\,\mathrm{mL\,min^{-1}}$ into the borehole. Inspection of the sample post-fracturing showed that the generated fracture cuts the full diameter of the sample; however, it did not propagate to the full height of the sample. The anticipated extent of the generated fracture shown in Fig. 3 is inferred from these observations. The defor-

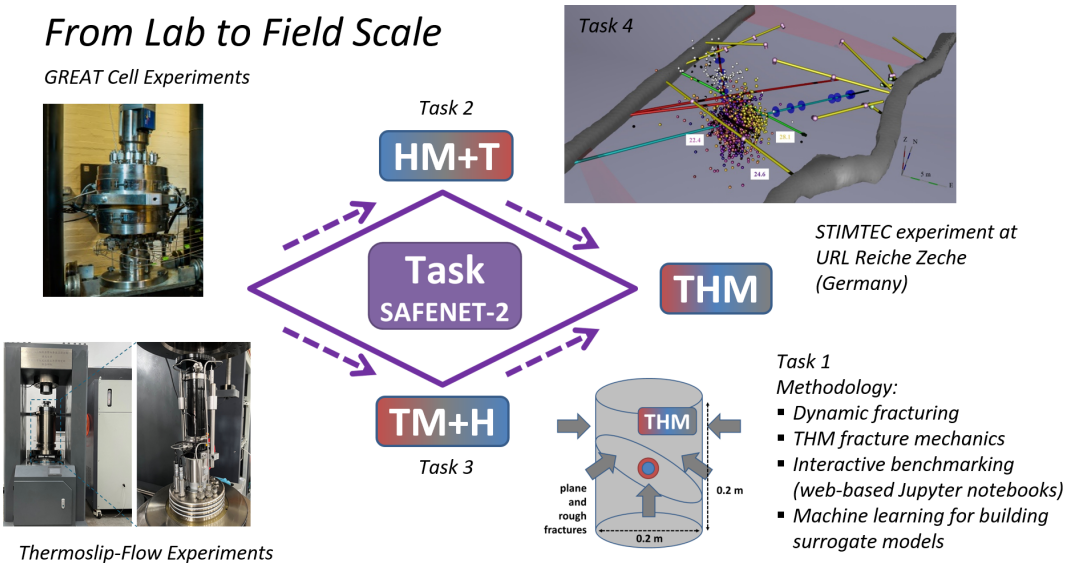

Figure 1. Concept of the SAFENET-2 Task of DECOVALEX 2027 following two routes towards THM processes and models for upscaling from the lab to field scale.

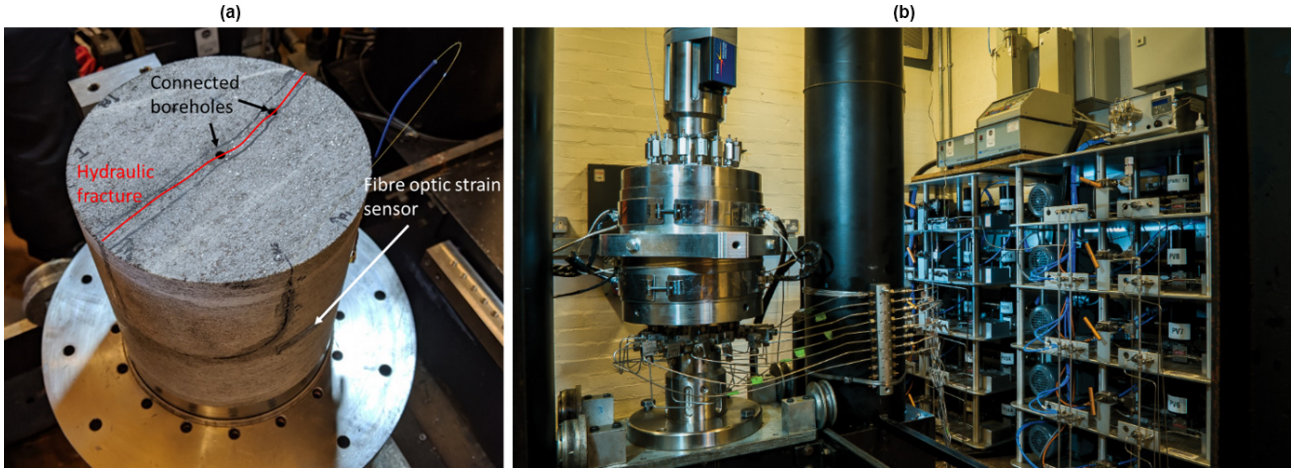

Figure 2. GREAT cell facility: **(a)** Freiberg gneiss sample after the fracture stage (the orientation of the foliation is highlighted, along with pre-existing sealed fracture that is interpreted as the youngest (and potentially weakest) discontinuity in the sample) and **(b)** experimental apparatus.

mation around the edge of the sample was recorded in terms of circumferential strain at 0.04 s intervals (25 Hz) during the fracturing process (Fig. 4). In addition, two dynamic fracture experiments and rotational deformation tests are available for the teams to model in granite under radially symmetric loading conditions of 8 and 12 MPa, with corresponding axial loads of 24 and 36 MPa. The dynamic deformation is recorded using the Luna fibre optic cable. The strain record is complete for the 12 MPa experiment, and part of the record is missing for the 8 MPa experiment.

(ii) *Fracture circulation experiments.* This experiment is designed to examine fluid flow in a fracture under a combination of different stress orientations and stress anisotropy ratios. Fluid flow through the fracture was facilitated by a second borehole drilled into the fracture developed within the Freiberg gneiss during the previous unconfined initiation experiments.

Figure 5a shows the schematic diagram of the fluid flow arrangements during the fracture circulation experiments. The extent of the hydraulic fracture generated during the uniaxial experiment is depicted in dark green, with the extent of the fracture available to fluid circulation in light blue. During the experiments, fluid was injected into the original borehole in the centre of the sample and was allowed to leave the sample via a second borehole positioned radially 50 mm

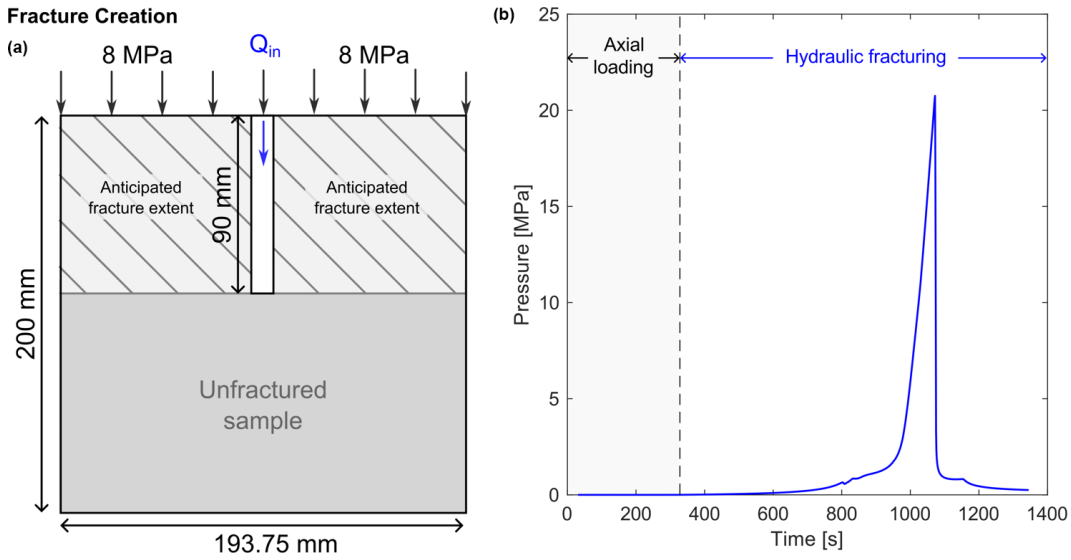

Figure 3. GREAT cell fracture initiation experiment: SAFENET-2-FE. **(a)** Schematic cross-section of the fractured cylindrical sample. **(b)** Fluid injection pressure recording during hydraulic fracturing.

away from the injection borehole. The fluid injection rate was $Q_i = 5\,\mathrm{mL\,min^{-1}}$, with fluid viscosity $\mu = 1.03 \times 10^{-3}\,\mathrm{Pa\,s}$ (close to the viscosity of pure water). Fluid was supplied via a pair of syringe pumps operating in constant flow rate mode.

After initial fracture creation experiments, two different stress rotation experiments were conducted. Rotation of the stress field around the sample with respect to the fracture allows us to investigate the relative impact of shear and normal stresses acting on the fracture surface on the fluid flow characteristics of the sample. The loading conditions for the GREAT cell pressure-exerting elements (PEEs) employ opposing banks of PEE triplets to apply σ_2 and σ_3. These are separated by single pairs of PEEs with a bridging stress σ_{bridge}, defined as the average of the intermediate and minimum principal stresses (Fig. 5b). Circumferential strains were measured continuously through rotation experiments to assess the influence of shear stress and stress orientation.

In the first stress rotation experiment, σ_2 and σ_3 were fixed at 12 and 6 MPa, respectively, and rotated in eight stages by 22.5° steps (stages 0 and 8 are identical in terms of applied stresses), with a bridging stress of 9 MPa (Fraser-Harris et al., 2020). The corresponding circumferential strains are shown in Fig. 6. The large blue arrows indicate the orientation of σ_2 (maximum horizontal stress) with respect to the fracture, and the small blue arrows indicate the orientation of σ_3 (minimum horizontal stress) with respect to the fracture. σ_1 is the axial stress. The stresses in each PEE pair during rotations are given in Table 1, where $\sigma_2 = \sigma_{2\mathrm{Max}}$.

In the second rotation experiment, the protocol was extended to include a series of sub-stages during each stress rotation whereby σ_2 is progressively increased from an initial axisymmetric stress state ($\sigma_2 = \sigma_3$) to $\sigma_2 = \sigma_1$ to investigate the impact of stress anisotropy. Before each incremental rotation of the stress field, a final sub-stage returns the sample to the initial axisymmetric stress state at the start of the rotation. Figure 7 shows the influence of increasing shear stress on fracture and surface strains. Increasing stresses σ_2 centred around the 135–315° axis were applied in stages from 6 to 12 MPa. As can be seen, the compressive strains decrease in response to progressive increases in σ_2, whereas dilational strains increase in the orthogonal direction (45–225° axis).

Fracture permeabilities have been estimated from both stress rotation experiments. No direct measure of the hydraulic aperture b [L] of the fracture was possible during either stress rotation experiment. In both experiments, the inferred planar nature of the fracture between the injection and fluid return boreholes justified the use of the cubic law for fracture permeability (Eq. 1a), from which the hydraulic aperture could be estimated.

$$Q_i = \frac{w b^3}{12\mu}\frac{\Delta P}{L} \tag{1a}$$

Consequently, the intrinsic permeability k [L^2] of the fracture could be obtained.

$$k = \frac{b^2}{12} \tag{1b}$$

Additionally, Q_i [$\mathrm{L^3\,T^{-1}}$] is the fluid injection–return rate, L [L] is the separation of the injection and return boreholes, μ [$\mathrm{M\,L^{-1}\,T^{-1}}$] is the fluid viscosity, and w [L] is the vertical height of the fracture. ΔP [$\mathrm{M\,L^{-1}\,T^{-2}}$] is the applied pressure differential. Throughout all rotations, the injection pumps were injected at the required pressure to maintain the prescribed flow rate against a fixed downstream pressure of 4.89 MPa as set via a back-pressure regulator fitted to the return fluid line.

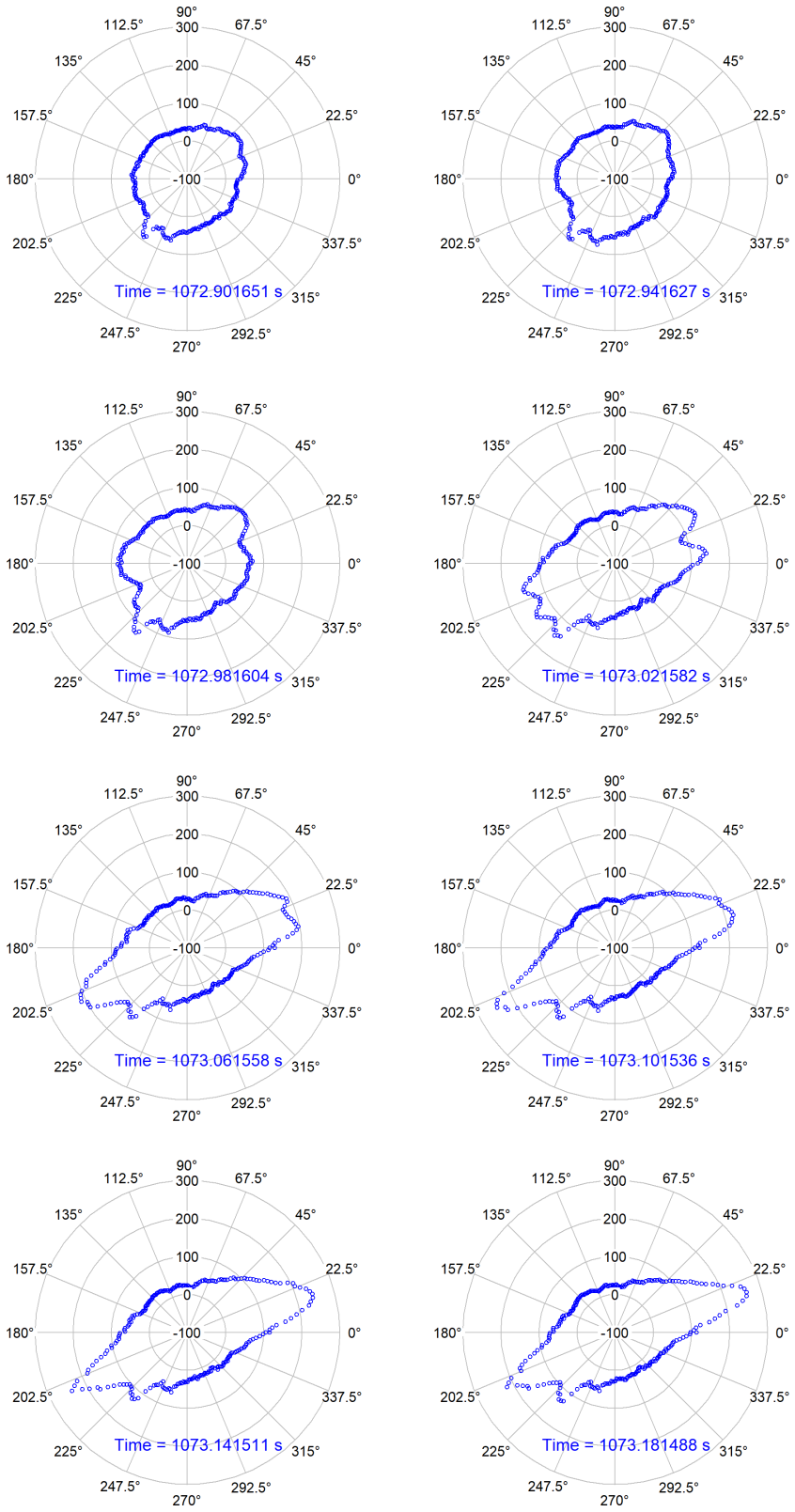

Figure 4. Circumferential strain measurements (in µstrain, i.e. $\varepsilon \times 10^{-6}$) beginning from $t = 1072.901651$ and $\Delta t \approx 0.04$ s intervals during hydraulic fracturing of the Freiberg gneiss sample. Given times in the individual subfigures correspond to the official time stamps of the experiment. Strains can be positive and negative as they are measurements relative to a starting point. Starting at -100 µstrain allows for a visual circular representation which should be more intuitive for the reader, namely a radar-type plot of the strain around the surface of the sample.

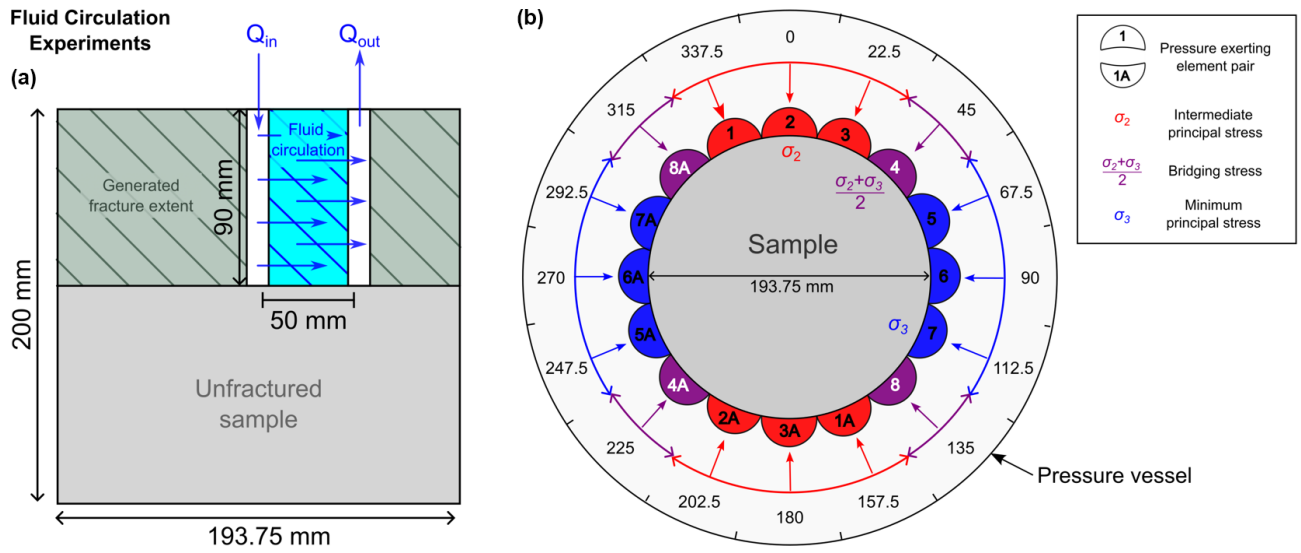

Figure 5. GREAT cell circulation experiment: SAFENET-2-CE. **(a)** Schematic of the fractured sample for the fluid circulation experiment. **(b)** Schematic of the rotating-stress-field application via PEE (pressure-exerting elements) triplets.

Table 1. The radial stress conditions employed in the fracture circulation experiments. The axial stress σ_1 is maintained at 12 MPa throughout the experiment. Sub-stages increment σ_2 from $\sigma_{2\text{Min}} = 6$ to $\sigma_{2\text{Max}} = 12$ MPa in 1 MPa increments. The bridging stress $\sigma_{\text{bridge}} = (\sigma_2 + \sigma_3)/2$ is incremented in steps of 0.5 MPa from 6 to 9 MPa. The column titled "stress" refers to the assignment of principal and bridging stresses prior to any rotations.

		Rotational step number (angle, θ)					
PEE pair	$\text{Stress}_{\theta=0}$	0 (0°)	1 (22.5°)	2 (45°)	⋯	7 (157.5°)	8 (180°)
Axial load	σ_1	12	12	12		12	12
1 & 1A	σ_3	6	6→9	6→12	⋯	6	6
2 & 2A	σ_3	6	6	6→9	⋯	6	6
3 & 3A	σ_3	6	6	6		6→9	6
4 & 4A	σ_{bridge}	6→9	6	6	Steps	6→12	6→9
5 & 5A	σ_2	6→12	6→9	6	3 to 6	6→12	6→12
6 & 6A	σ_2	6→12	6→12	6→9		6→12	6→12
7 & 7A	σ_2	6→12	6→12	6→12	⋯	6→9	6→12
8 & 8A	σ_{bridge}	6→9	6→12	6→12	⋯	6	6→9

Figure 8a shows the estimated permeabilities from the experiments where σ_2 was incrementally increased during each rotation as a function of mean modelled normal stress. Permeability is seen to decrease with increasing normal stresses in the plane of the fracture. Likewise, Fig. 8b shows the modelled maximum shear stress in the plane of the fracture. The normal and shear stresses on the fracture plane are not directly measured but rather are interpreted from the directional stress applied to the sample and the orientation of the fracture plane in this stress field. Therefore, they are denoted as modelled stresses. Again, permeability appears to decrease with increasing maximum resolved shear stress; however, the sensitivity of the change in permeability appears to be more pronounced than for the resolved normal stress.

2.2.2 Thermoslip-flow lab-scale data

The concept of the thermoslip-flow test is illustrated in Fig. 9. Using the customised fault shear flow testing machine at Chongqing University, an inclined natural rock fracture with roughness cutting through a cylindrical rock specimen (50 mm diameter × 100 m length) is initially loaded close to criticality. The specimen is then heated by heating the confining oil. During the heating period, σ_3 will be constant, while thermal expansion is restricted in the axial direction. As a result, thermal stress (σ_T) will be generated and added to σ_1, as shown in Fig. 9a. Thermoslip occurs when the σ_1 is high enough to reach the Mohr–Coulomb failure criterion.

It is generally assumed that shear dilation of rough fractures will result in an increase in permeability. Plans are therefore in place to evaluate the hydraulic performance be-

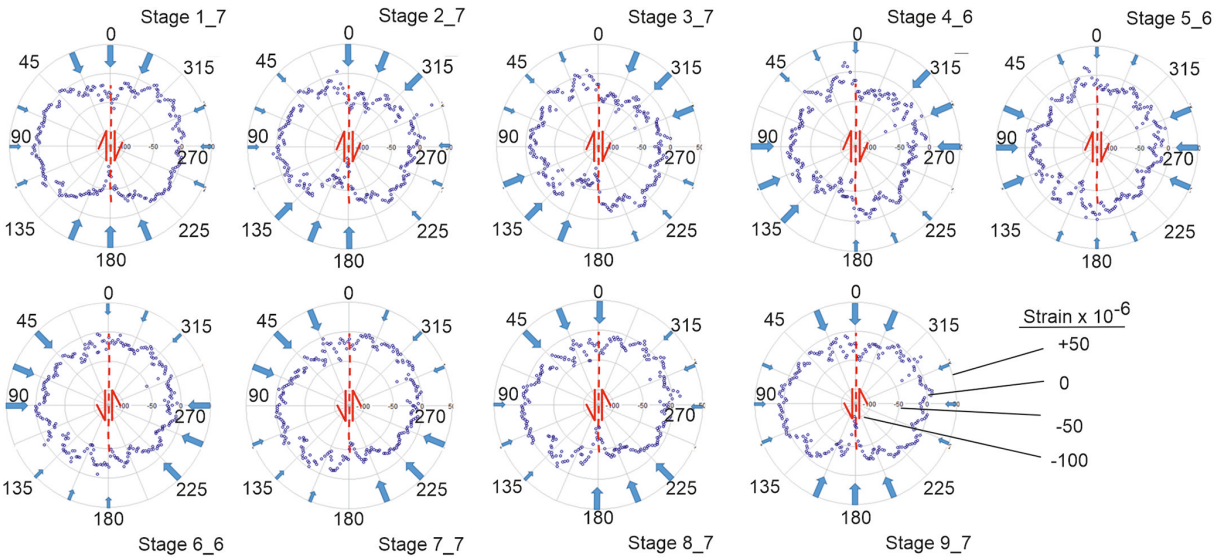

Figure 6. Circumferential strains during the first stress rotation experiment. Maximum stress $\sigma_1 = 12$ MPa, and minimum stress $\sigma_3 = 6$ MPa. Intermediate stress $\sigma_2 = 12$ MPa is rotated around the sample in eight stages. In this case, the results have not been normalised to stage 3_1; see Fig. 7.

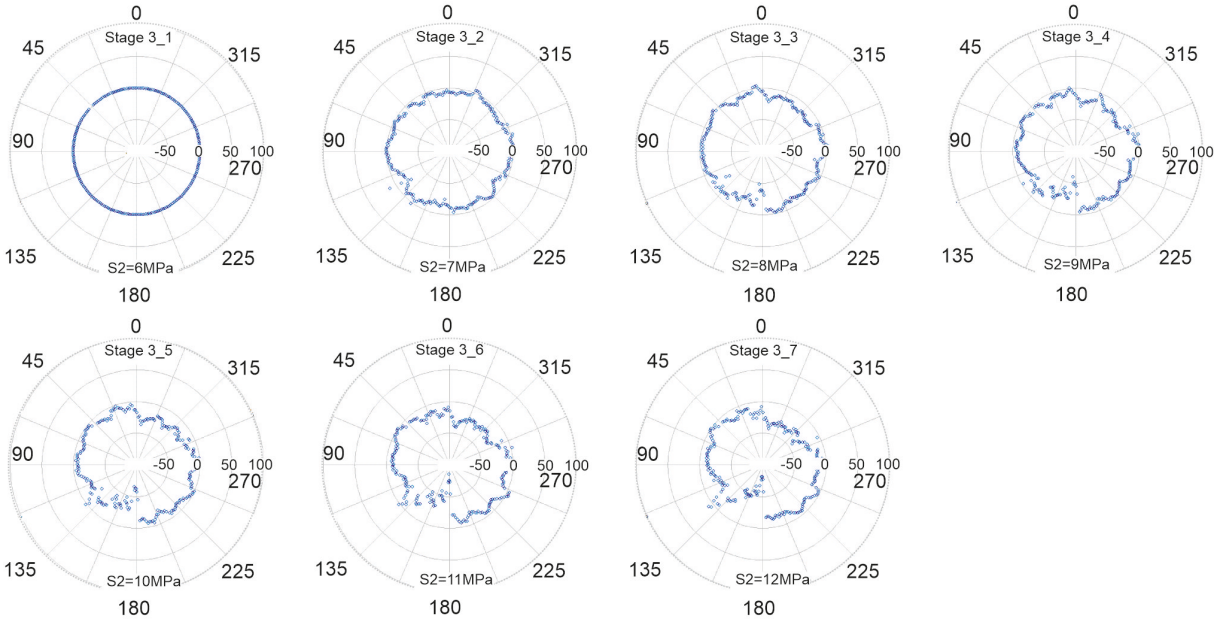

Figure 7. Circumferential strains (in µstrain, i.e. $\varepsilon \times 10^{-6}$) during the second stress rotation experiment, with increasing σ_2 stresses around 135–315° axis ($\sigma_3 = 6$ MPa $\sigma_1 = 12$ MPa in all cases, all normalised to stage 3_1). Strains can be positive and negative strains as they are measurements relative to a starting point. Starting at -100 µstrain allows for a visual circular representation which should be more intuitive for the reader, namely a radar-type plot of the strain around the surface of the sample.

fore and after thermoshearing. This was not considered in the last phase of SAFENET, where thermoshear tests were conducted under dry conditions (Sun et al., 2021, 2023, 2025). Fluid is injected through the fluid inlet at the bottom and flows through the fracture to the fluid outlet, as shown in Fig. 9b. The pressures at the inlet and outlet are monitored. The fluid flow characteristics before and after thermally induced fracture slip are analysed. In this way, the coupled TM+H behaviour of a rock fracture is studied. The data obtained from the thermoslip-flow test in Fig. 9b will be used for numerical modelling benchmarking.

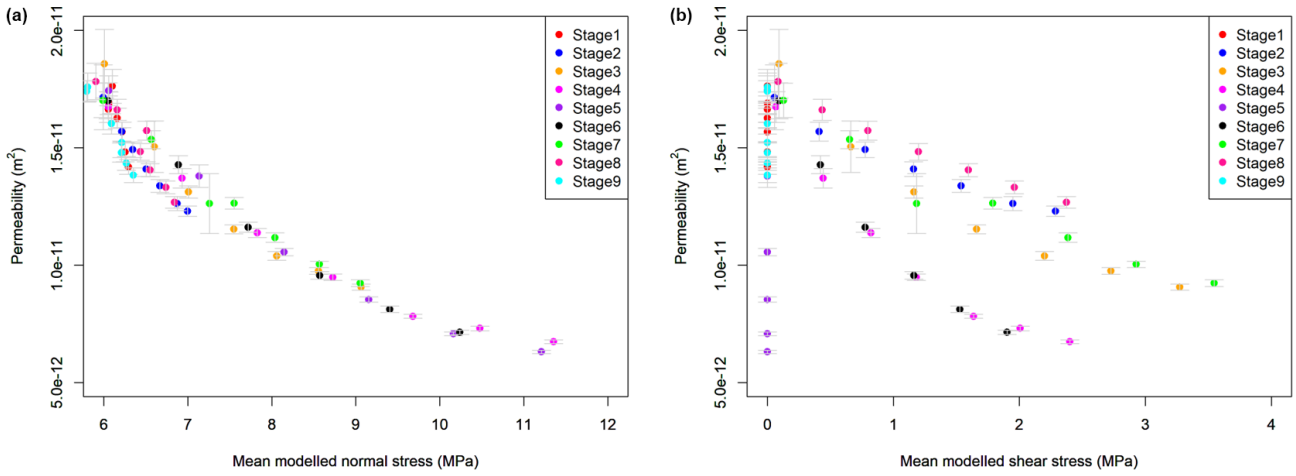

Figure 8. Variation in fracture permeability as a function of normal **(a)** and shear stresses **(b)**.

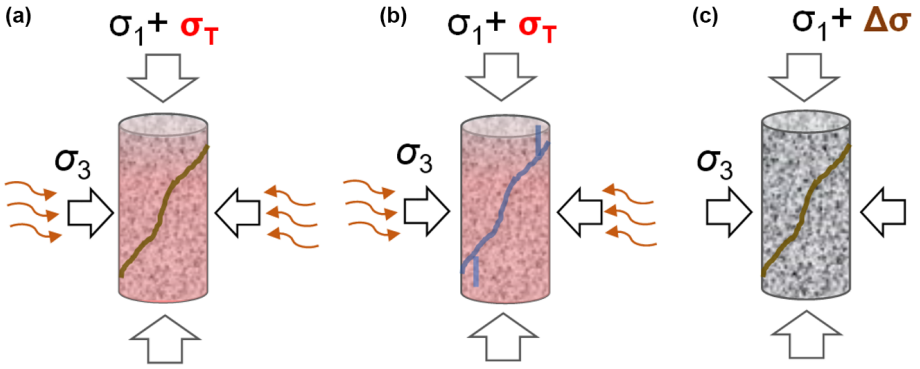

Figure 9. Schematic diagram of the experiments: **(a)** thermoshearing test (or thermoslip test), **(b)** thermoslip-flow test for the modelling benchmarking and **(c)** mechanical shear test.

In addition, it is planned that the thermoshearing test (TM) without fluid interaction and the mechanical shear test (M) without thermal or fluid interaction will be used for a comparison of shear behaviour, as shown in Fig. 9a and b. To ensure comparability, we plan to use a reproducible rough fracture with nearly the same topography in the M, TM and TM+H experiments. The fracture will be produced using a digital stone-engraving machine with a maximum location accuracy of 10 µm.

2.2.3 STIMTEC in situ experiments

The experimental basis at the field scale is provided by the STIMTEC experiment in the teaching and research mine Reiche Zeche, where stimulation tests with periodic pumping tests and high-resolution seismic monitoring have been conducted (Boese et al., 2021, 2022; Blanke et al., 2023; Boese et al., 2023). Statistical properties for the characterisation of the stress field heterogeneity have been analysed by Jimenez-Martinez and Renner (2023). Investigations of the main hydro-mechanical phenomena and of the characteristics of the in situ experiment have been carried out by Schmidt et al. (2021, 2023) and also within the GeomInt project (Kolditz et al., 2021). Together with laboratory experimental data, the STIMTEC experiment will provide a basis for upscaling fracture models from the laboratory to field scale with respect to hydro-mechanically induced fracture processes.

2.3 Modelling approach – steps of the DECOVALEX Task

All DECOVALEX Tasks are organised into steps. The SAFENET-2 Task is divided into two groups: (i) conceptual work (steps 1 and 5) and (ii) experimental analyses of lab and field experiments (steps 2, 3 and 4).

- Step 1: benchmarking (Sect. 2.3.1)
- Step 2: GREAT cell experiments (Sect. 2.3.2)
- Step 3: thermoslip experiments (Sect. 2.3.3)
- Step 4: STIMTEC experiments (Sect. 2.3)

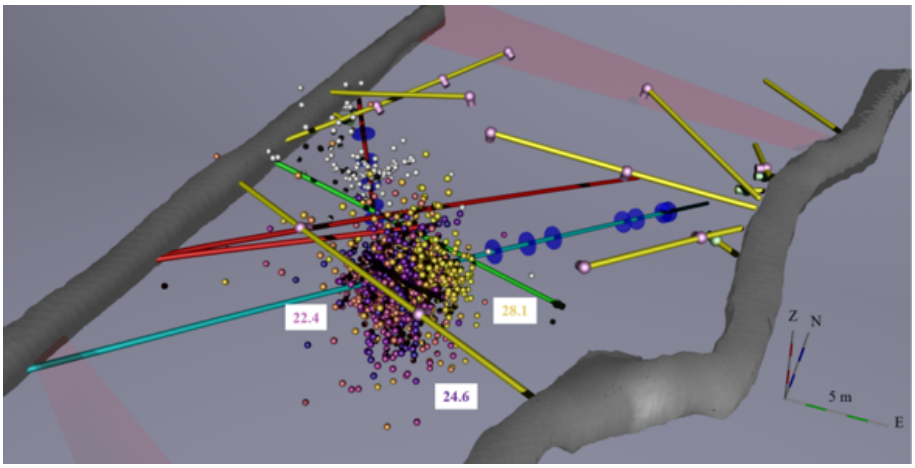

Figure 10. Setup of boreholes in the STIMTEC field experiment in the underground teaching and research mine Reiche Zeche at Technische Universität Bergakademie Freiberg (courtesy of Caroline Boese). The spheres indicate the location of acoustic emissions induced during various stages of fluid injection.

– Step 5: synthesis (Sect. 2.3.4)

2.3.1 Step 1: benchmark simulations

The main objective of step 1 is to provide a suite of benchmarks for SAFENET-2. These benchmarks will cover the basic features of the GREAT cell, Chongqing and STIMTEC experiments in a simplified way so that the modelling teams can test their methods and codes to see if they are, in principle, able to simulate the laboratory and in situ experiments. The benchmark suite will therefore provide a common basis for the modelling teams and allow typical benchmarking exercises such as grid convergence tests to prove correct discretisation for simulating the fracture processes with sufficient accuracy. The benchmark suite will be made available as an open-science contribution via interactive Jupyter notebooks to encourage more teams not currently involved in DECOVALEX to participate in these benchmarking exercises and to create an easily findable, accessible, interoperable and reproducible reference.

Step 1.1. Figure 11 shows the benchmark suite for THM fracture processes that is featured by the GREAT cell experiments but that also serves to benchmark TM and TM+H models for the thermoslip experiments. The basic idea is to mimic fracture processes in a rotating stress field. The HM version has already been completed as part of SAFENET-1 (Mollaali et al., 2023). The THM includes thermal processes by externally heating the rock samples to mimic different thermal boundary conditions (e.g. depth-dependent geothermal temperatures).

Step 1.2: thermoslip-flow benchmarks. The modelling exercises are divided into the following sub-steps according to the main processes: M, TM, HM and THM (Fig. 12) experiments. Since the main features of the experiments can also be simulated in plane–strain models, we start the modelling

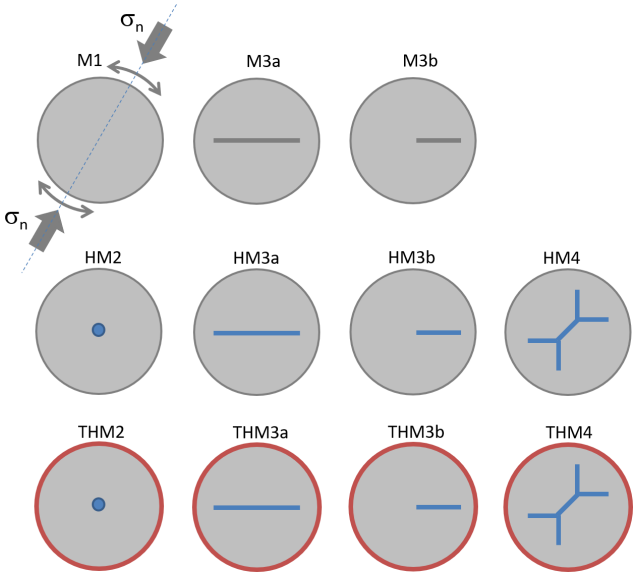

Figure 11. GREAT cell THM benchmarking suite.

exercises in 2D and then continue in 3D in step 3 (Fig. 16, right). Additionally, models for both plane and rough fractures will examined.

Step 1.3. The concept of the STIMTEC benchmark is a single fracture embedded in a block of gneiss. The fracture is intended to represent one of the larger discontinuities observed in the research mine (i.e. realistic fracture orientation, Fig. 13). Realistic in situ stresses are imposed by appropriate stress boundary conditions. The basic idea of this benchmark test is to qualitatively reproduce the hydraulic pressure responses to the various stimulation phases during the STIMTEC experiment, i.e. *p* test, frac test, re-fracs, step-rate test, and shut-in and periodic-pumping tests (see Sect. 2.3).

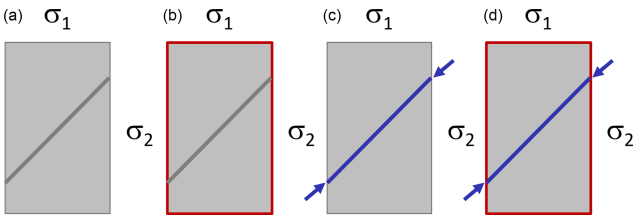

Figure 12. Benchmarking exercises for the thermoslip-flow cell experiments: investigation of the individual mechanical (M) and mechanical coupled processes with increasing complexity (TM > HM > THM) (from left to right).

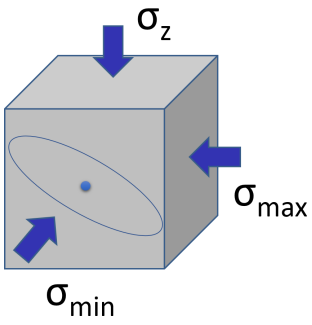

Figure 13. STIMTEC benchmark concept.

2.3.2 Step 2: GREAT cell test case simulation

Three experiments conducted with gneiss and granite samples are available for simulation. A "large" natural heterogeneous foliated Freiberg gneiss sample is hydraulically fractured under axial-load confined conditions and unconfined radial conditions – the fracture is free to form according to the influence of foliations:

- process – dynamic fracture formation, unconfined;
- material – Freiberg gneiss;
- conditions – $\sigma_1 = 8$ MPa, $\sigma_2 = \sigma_3 = 0$, $\varnothing = 200$ mm;
- experimental data – time-dependent fluid pressure, surface deformation @100 Hz, dynamic fracture growth recorded.

Two "large" granite samples are hydraulically fractured under axial-load confined conditions and confined radial conditions. Two boreholes are drilled into the fracture to facilitate fluid flow measurements, and estimates of permeability under different stress and fluid flow conditions are available:

- process – dynamic fracture formation, confined ×2;
- material – G603 granite;
- conditions – $\sigma_1 = 24$ MPa, $\sigma_2 = \sigma_3 = 8$ MPa, $\varnothing = 200$ mm;
- conditions – $\sigma_1 = 32$ MPa, $\sigma_2 = \sigma_3 = 12$ MPa, $\varnothing = 200$ mm;
- experimental data – time-dependent fluid pressure, surface deformation @100 Hz, dynamic fracture growth recorded.

The modelling exercises are divided into the following sub-steps according to the two main experiments: hydraulic fracturing (sub-step 2.1) and flow circulation (sub-step 2.2). In sub-step 2.1, the hydraulic-fracturing process is simulated according to the experimental conditions (Fig. 14(HM2.1a)). In sub-step 2.2, the flow circulation experiment is modelled in two versions according to the rotating stress field (sub-step 2.2a; Fig. 14, HM2.2a1) and the stepwise increase in stress in the direction of the fracture orientation (sub-step 2.2b; Fig. 14, HM2.2a2). Since the main features of the experiments can also be simulated in plane–strain models, we will start the modelling exercises in 2D and continue them in 3D (Fig. 14(HM3)).

2.3.3 Step 3: Thermoslip-flow test case simulation

Granite cores from the Beishan Underground Research Laboratory will be used in the experiments. For details about the physical and mechanical properties, we refer to Chen et al. (2023); Yi et al. (2024). The experiment team of Chongqing University will select a granite core containing a typical rough fracture or natural fracture (Fig. 15). The surface topography of the fracture will be obtained using a high-resolution optical 3D scanner, and the initial contact conditions between the top and bottom can be investigated using a CT scan (Fig. 15a). In situ stress and heating conditions will be decided based on a pre-modelling procedure, which will give details about the distributions of temperature and thermal stress inside the granite specimen (Sun et al., 2024). The surface profile data of the fracture, basic physical and mechanical properties of the granite, and heating boundaries were delivered during the second DECOVALEX workshop in October 2024. With the specimen properties and given heating conditions, benchmarking teams will conduct numerical modelling to estimate the temperature, thermal stress and shear behaviour of the rough fractures. This process is defined as a blind prediction. The test results include but are not limited to (1) asperity damage, (2) interlock, (3) slip pattern and (4) permeability change. Suggested items on the benchmarking list are as follows:

- temperature and thermal stress distribution
- slip displacement and slip pattern
- shear dilation and permeability change
- asperity damage distribution
- influence of interlock.

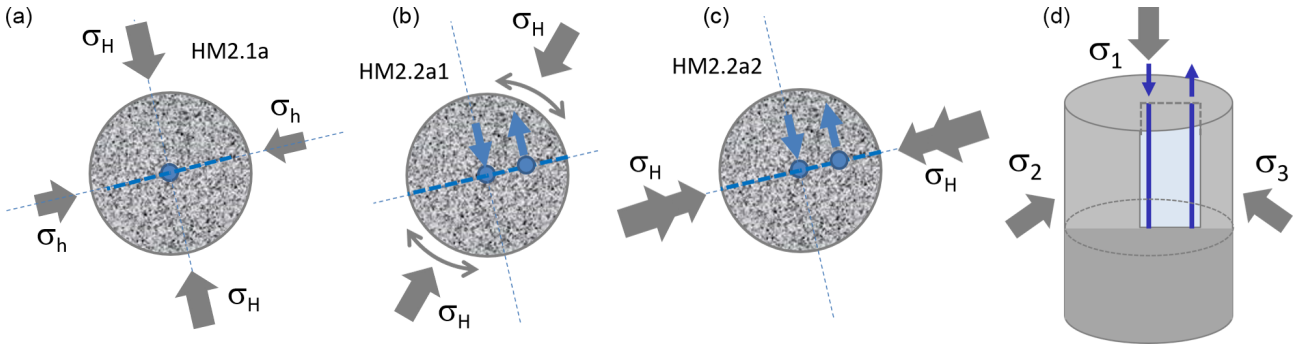

Figure 14. Modelling exercises for the GREAT cell experiments: HM2.1, HM2.2a, HM2.2b, HM3.1 and HM3.2 (from left to right).

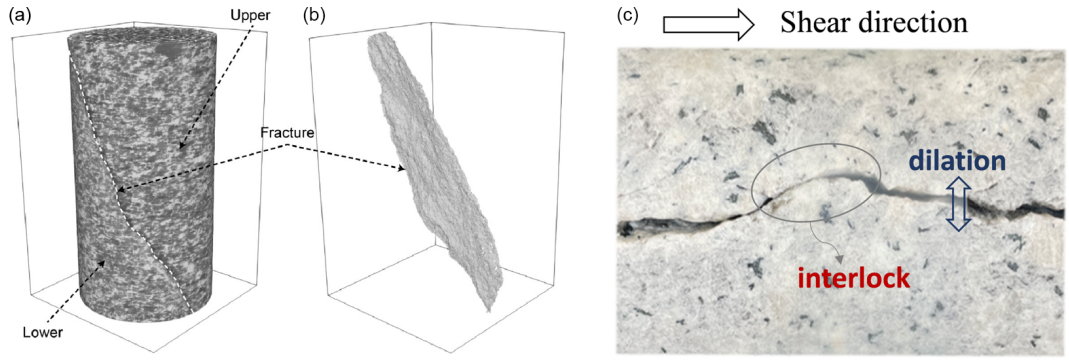

Figure 15. Granite specimen used for experiments: **(a)** the inclined through-going rough fracture in a granite cylinder, **(b)** an example showing the upper fracture climbing over the lower one in an originally interlocked granite specimen. Shear dilation occurred as a result of shearing.

In particular, we are curious about the effect of interlock on the slip behaviour, such as the slip pattern and shear dilation (Fig. 15b). The step-2 test case simulation will commence in late 2025.

Since the main features of the experiments can also be simulated in plane–strain models, we start with the benchmarking exercises in 2D and then continue in 3D (Fig. 16). Additionally, models for both plane and rough fractures will be examined.

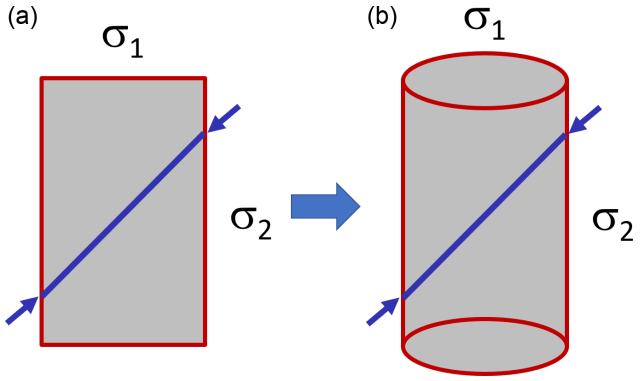

Figure 16. Extending thermoslip-flow cell models from 2D benchmarks **(a)** to 3D real samples **(b)**.

Step 4: STIMTEC in-situ experiments

Hydraulic injection and stimulation results will be analysed to characterise in situ fracture permeabilities. Acoustic emission data will be used to constrain fracture mechanics models. The pressure response to the successive hydraulic test stages is shown in Fig. 17: (i) p test, (ii) hydraulic fracturing (frac), (iii) re-fracturing (re-fracs), (iv) step-rate tests, (v) shut-in and (vi) periodic-pumping test.

After benchmarking the typical hydraulic features of the STIMTEC experiment, step 3 is to characterise the in situ hydraulic behaviour, i.e. to identify the hydro-mechanical rock properties. The teams can choose their preferred fracture network model; a suggested starting point is the main hydraulic feature as shown in Fig. 18.

2.3.4 Step 5: synthesis and open sciences

Results will be synthesised for the evaluation of numerical methods, model upscaling from the lab to field scale and the applicability of the methodology for related application areas

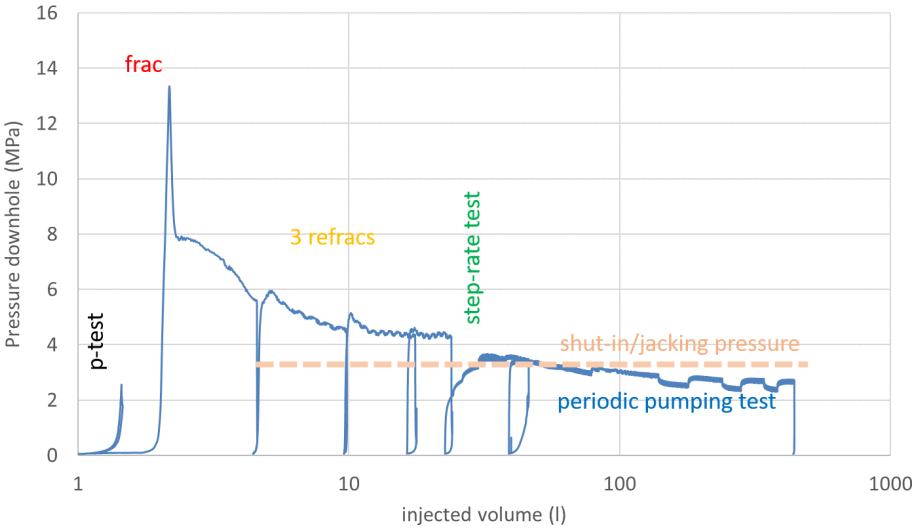

Figure 17. STIMTEC field experiment: hydraulic in situ testing.

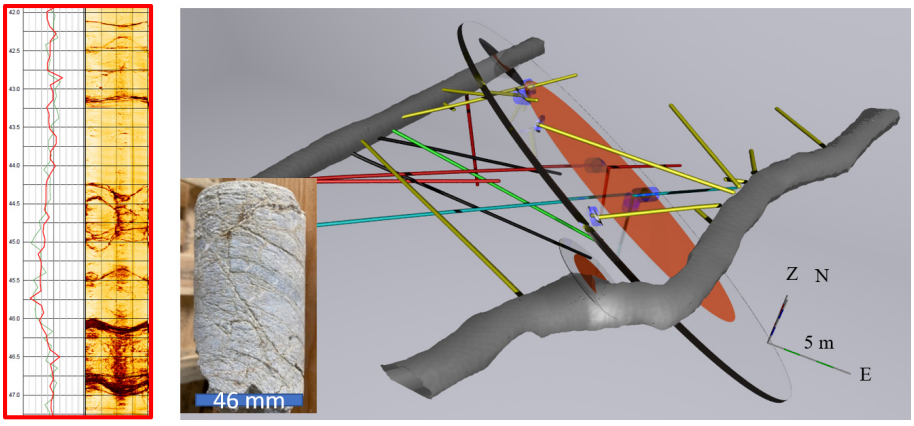

Figure 18. STIMTEC field experiment: the highlighted disc represents the orientation of an assumed natural discontinuity (Boese et al., 2022, 2023).

(e.g. geothermal reservoirs in crystalline rock). SAFENET-2 will actively contribute to open-science action in nuclear waste management (Kolditz et al., 2023; Lehmann et al., 2024), e.g. by providing benchmarking tools via an interactive web platform.

3 Conclusions

We presented the intention, concept and related experimental facilities of SAFENET-2, a Task of the new DECOVALEX 2027 project. After a short introduction of the intention and concept of the Task, the experimental facilities and basics were described. Rock samples will be analysed from underground research laboratories in Germany (Reiche Zeche) and China (Beishan). SAFENET-2 will, again, follow two paths towards fully coupled thermo-hydro-mechanical (THM) fracture processes: (i) HM+T, extending HM processes to include thermal processes, and (ii) TM+H, extending thermo-mechanical processes to include hydraulic processes. The numerical basis for fully coupled THM processes will be provided by a set of benchmarks for model and code testing. In addition, typical benchmarks will be designed to capture the main features of the new GREAT cell and thermoslip-flow experiments conducted at the rock mechanics laboratories in Edinburgh and Chongqing, respectively. Finally, the in situ STIMTEC experiments are studied to demonstrate the scalability of the models for field experiments. Table 2 shows the tentative time schedule for the SAFENET-2 Task.

This paper is dedicated to the special issue of SAND, “Trust in Models”. Models will play an important role in the deep geological disposal of radioactive waste as predictions of the possible evolution of repositories are a rigorous part of the safety assessment. Therefore, model valida-

Table 2. Time schedule for the SAFENET-2 Task.

SAFENET-2 schedule			2024				2025				2026				2027				
Step1		Benchmarking																	
	1.1	GREAT cell																	B1
	1.2	Thermoslip-flow cell experiments																	B2
	1.3	STIMTEC experiments																	B3
		Paper ideas					B1		B2	B3									
Step2		GREAT experiments																	
	2.1	Hydraulic fracturing																	G1
	2.2a	Circulation flow experiment																	
	2.2b	Circulation flow experiment																	G2
	2.3	3D version																	G3
										G1		G2		G3					
Step 3		Thermoslip-flow cell experiments																	
	3.1	M process																	
	3.2	TM process																	
	3.3	HM process																	
	3.4	THM process																	T1
	3.5	3D version																	T2
		Paper ideas												T1		T2			
Step 4		STIMTEC experiments																	
	4.1																		S1
		Paper ideas															S1		
Step 5		Synthesis																	
	5.1																		S2
		Paper ideas																S2	
		Workshops	WS1		WS2		WS3		WS4		WS5		WS6		WS7		WS8		

tion is of utmost importance for the credibility of the modelling process in radioactive waste disposal. SAFENET contributes to this goal in several ways by (i) providing a new experimentally based benchmark suite for fracture models in crystalline rock; (ii) analysing new unique experimental data for the description of THM processes in different crystalline rock samples; and (iii) applying validated models resulting from (i) and (ii) to the analysis of in situ experiments at the field scale, thus also contributing to a better understanding of the upscaling behaviour in crystalline rock masses. This paper presents the introduction and detailed description of the second SAFENET-2 Task within the DECOVALEX 2027 project. The progress of the team's work will be reported in subsequent publications and in the synthesis paper with the main research results at the end of the Task (Table 2).

Code availability. SAFENET relies on both open-source and commercial code. For the former, source codes are available from https://doi.org/10.5281/zenodo.13685289 (Bilke et al., 2025). For both, the corresponding input files are made available on the DECOVALEX website.

Data availability. Experimental data are made available on the DECOVALEX website (http://www.decovalex.org; The University of Edinburgh and Chongqing University, 2025).

Author contributions. OK: research concept, benchmarking concept, main writing; CM: research concept, experimental concept and data, paper writing; JSY: research concept, numerical simulation; JR: experimental concept and data; LZ: experimental data, paper writing; AFH: experimental data; MC: experimental data; SG: experimental data; JW: rock samples and experimental data; MM: benchmarking concept, numerical simulation.

Competing interests. The contact author has declared that none of the authors has any competing interests.

Disclaimer. Publisher's note: Copernicus Publications remains neutral with regard to jurisdictional claims made in the text, published maps, institutional affiliations, or any other geographical representation in this paper. While Copernicus Publications makes every effort to include appropriate place names, the final responsibility lies with the authors.

Special issue statement. This article is part of the special issue "Trust in Models". It is a result of the "Trust in Models" workshop series, Berlin, 2022–2025, Germany.

Acknowledgements. DECOVALEX (https://decovalex.org, last access: 14 March 2025) is an international research project comprising participants from industry, government and academia, focusing on the development of understanding, models and codes in complex coupled problems in subsurface geological and engineering applications; DECOVALEX 2027 is the current phase of the project. The authors appreciate and thank the DECOVALEX 2027 funding organisations, Andra, BASE, BGE, BGR, CAS, CNSC, COVRA, US DOE, ENRESA, ENSI, JAEA, KAERI, NWMO, RWM, SÚRAO, SSM, and Taipower, for their financial and technical support of the work described in this paper. BGR is subordinate to the German Federal Ministry for Economic Affairs and Climate Action (BMWK). The statements made in this paper are, however, solely those of the authors and do not necessarily reflect those of the funding organisations. Furthermore, this work has been co-financed within the framework of EURAD, the European Joint Programme on Radioactive Waste Management (grant no. 847593). Financial support from the UK Engineering and Physical Sciences Research Council (EPSRC) for the project "Smart Pumping for Subsurface Engineering" (grant no. EP/S005560/1) is gratefully acknowledged for the provision of experimental data relating to the GREAT cell. We wish to thank the editorial team of the *Safety of Nuclear Waste Disposal* journal for their dedication in handling the paper and creating a productive atmosphere during the revision process.

Financial support. This research has been supported by the European Commission, Euratom Research and Training Programme (grant no. 847593), and the Engineering and Physical Sciences Research Council (grant no. EP/S005560/1).

Review statement. This paper was edited by Carlo Dietl and reviewed by Eleonora Crisci and one anonymous referee.

References

Bang, H.-T., Yoon, S., and Jeon, H.: Application of machine learning methods to predict a thermal conductivity model for compacted bentonite, Ann. Nucl. Energy, 142, 107395, https://doi.org/10.1016/j.anucene.2020.107395, 2020.

BASE: Quo Vadis – Künstliche Intelligenz in der nuklearen Entsorgung, Workshop proceedings, Bundesamt für die Sicherheit der nuklearen Entsorgung (BASE), 10623 Berlin, Wegelystrasse 8, 2023.

Bilke, L., Flemisch, B., Kalbacher, T., Kolditz, O., Helmig, R., and Nagel, T.: Development of Open-Source Porous Media Simulators: Principles and Experiences, Transport Porous Med., 130, 337–361, https://doi.org/10.1007/s11242-019-01310-1, 2019.

Bilke, L., Naumov, D., Wang, W., Fischer, T., Kiszkurno, F. K., Lehmann, C., Jäschke, M., Zill, F., Buchwald, J., Grunwald, N., Kessler, K., Aubry, L., Dörnbrack, M., Nagel, T., Ahrendt, L., Kaiser, S., and Meisel, T.: OpenGeoSys. Version: 6.5.4, Zenodo [code], https://doi.org/10.5281/zenodo.13685289, 2025.

Birkholzer, J. T., Bond, A. E., and Tsang, C.-F.: The DECOVALEX international collaboration on modeling of coupled subsurface processes and its contribution to confidence building in radioactive waste disposal, Hydrogeol. J., 32, 1295–1305, https://doi.org/10.1007/s10040-024-02799-7, 2024.

Blanke, A., Boese, C. M., Dresen, G., Bohnhoff, M., and Kwiatek, G.: Metre-scale damage zone characterization using S-coda waves from active ultrasonic transmission measurements in the STIMTEC project, URL Reiche Zeche, Germany, Geophys. J. Int., 233, 1339–1355, https://doi.org/10.1093/gji/ggad003, 2023.

Boese, C., Kwiatek, G., Dresen, G., Fischer, T., and Renner, J.: AE-type hydrophone performance during the STIMTEC and STIMTEC-X hydraulic stimulation campaigns at Reiche Zeche Mine, Germany, vol. 4, https://www.scopus.com/inward/record.uri?eid=2-s2.0-85123058188&partnerID=40&md5=5b69c9badb6dbcb7bc06ff8f6bec68cc (last access: 14 March 2025), 2021.

Boese, C. M., Kwiatek, G., Fischer, T., Plenkers, K., Starke, J., Blümle, F., Janssen, C., and Dresen, G.: Seismic monitoring of the STIMTEC hydraulic stimulation experiment in anisotropic metamorphic gneiss, Solid Earth, 13, 323–346, https://doi.org/10.5194/se-13-323-2022, 2022.

Boese, C. M., Kwiatek, G., Plenkers, K., Fischer, T., and Dresen, G.: Performance Evaluation of AE Sensors Installed Like Hydrophones in Adaptive Monitoring Networks During a Decametre-Scale Hydraulic Stimulation Experiment, Rock Mech. Rock Eng., 56, 6983–7001, https://doi.org/10.1007/s00603-023-03418-9, 2023.

Booker, J. and Savvidou, C.: Consolidation around a point heat source, Int. J. Numer. Anal. Met., 9, 173–184, https://doi.org/10.1002/nag.1610090206, 1985.

Breitkreutz, H., Mayr, J., Bleher, M., Seifert, S., and Stöhlker, U.: Identification and quantification of anomalies in environmental gamma dose rate time series using artificial intelligence, J. Environ. Radioactiv., 259–260, 107082, https://doi.org/10.1016/j.jenvrad.2022.107082, 2023.

Buchwald, J., Kolditz, O., and Nagel, T.: Design-of-Experiment (DoE) based history matching for probabilistic integrity analysis – A case study of the FE-experiment at Mont Terri, Reliability Engineering and System Safety, 244, 109903, https://doi.org/10.1016/j.ress.2023.109903, 2024.

Chan, T., Christiansson, R., Boulton, G., Ericsson, L., Hartikainen, J., Jensen, M., Mas Ivars, D., Stanchell, F., Vistrand, P., and Wallroth, T.: DECOVALEX III BMT3/BENCHPAR WP4: The thermo-hydro-mechanical responses to a glacial cycle and their potential implications for deep geological disposal of nuclear fuel waste in a fractured crystalline rock mass, Int. J. Rock Mech. Min., 42, 805–827, https://doi.org/10.1016/j.ijrmms.2005.03.017, 2005.

Chaudhry, A., Buchwald, J., Kolditz, O., and Nagel, T.: Consolidation around a point heat source (correction and verification), Int. J. Numer. Anal. Met., 43, 2743–2751, https://doi.org/10.1002/nag.2998, 2019.

Chen, L., Zhao, X., Liu, J., Ma, H., Wang, C., Zhang, H., and Wang, J.: Progress on rock mechanics research of Beishan granite for geological disposal of high-level radioac-

tive waste in China, Rock Mechanics Bulletin, 2, 100046, https://doi.org/10.1016/j.rockmb.2023.100046, 2023.

Claret, F., Dauzeres, A., Jacques, D., Sellin, P., Cochepin, B., De Windt, L., Garibay-Rodriguez, J., Govaerts, J., Leupin, O., Mon Lopez, A., Montenegro, L., Montoya, V., Prasianakis, N. I., Samper, J., and Talandier, J.: Modelling of the long-term evolution and performance of engineered barrier system, EPJ Nuclear Sciences and Technologies, 8, 41, https://doi.org/10.1051/epjn/2022038, 2022.

Flynn, J., Burns, W., Mertz, C., and Slovic, P.: Trust as a Determinant of Opposition to a High-Level Radioactive Waste Repository: Analysis of a Structural Model, Risk Anal., 12, 417–429, https://doi.org/10.1111/j.1539-6924.1992.tb00694.x, 1992.

Fraser-Harris, A., McDermott, C., Couples, G., Edlmann, K., Lightbody, A., Cartwright-Taylor, A., Kendrick, J., Brondolo, F., Fazio, M., and Sauter, M.: Experimental Investigation of Hydraulic Fracturing and Stress Sensitivity of Fracture Permeability Under Changing Polyaxial Stress Conditions, J. Geophys. Res.-Sol. Ea., 125, e2020JB020044, https://doi.org/10.1029/2020JB020044, 2020.

Fraser-Harris, A., McDermott, C., Lightbody, A., Edlmann, K., and Sauter, M.: The influence of intermediate principal stress magnitude and orientation on fracture fluid flow characteristics of a fractured crystalline rock, in preparation, 2025.

Frühwirt, T., Pötschke, D., and Konietzky, H.: Simulation of direct shear tests using a forces on fracture surfaces (FFS) approach, Environ. Earth Sci., 80, 1–10, 2021.

Hu, G. and Pfingsten, W.: Data-driven machine learning for disposal of high-level nuclear waste: A review, Ann. Nucl. Energy, 180, 109452, https://doi.org/10.1016/j.anucene.2022.109452, 2023.

Hu, G., Schoenball, M., and Pfingsten, W.: Machine learning-assisted heat transport modelling for full-scale emplacement experiment at Mont Terri underground laboratory, Int. J. Heat Mass Tran., 213, 124290, https://doi.org/10.1016/j.ijheatmasstransfer.2023.124290, 2023.

Hu, G., Prasianakis, N., Churakov, S. V., and Pfingsten, W.: Performance analysis of data-driven and physics-informed machine learning methods for thermal-hydraulic processes in Full-scale Emplacement experiment, Appl. Therm. Eng., 245, 122836, https://doi.org/10.1016/j.applthermaleng.2024.122836, 2024.

Jacques, D., Kolditz, O., Szőke, I., Churakov, S. V., García, D., Laloy, E., Montoya, V., Prasianakis, N. I., and Samper, J.: Digitalization and digital twins in long term management of radioactive waste, Proceedings of the ASME 2023 International Conference on Environmental Remediation and Radioactive Waste Management, ASME 2023 International Conference on Environmental Remediation and Radioactive Waste Management, 3–6 October 2023, Stuttgart, Germany, V001T10A007, ASME, https://doi.org/10.1115/ICEM2023-110268, 2023.

Jimenez-Martinez, V. and Renner, J.: Statistical approach to characterize stress field heterogeneity, in: Proceedings of the 57th US Rock Mechanics/Geomechanics Symposium, paper presented at the 57th U.S. Rock Mechanics/Geomechanics Symposium, June 2023, Atlanta, Georgia, USA, https://doi.org/10.56952/ARMA-2023-0641, 2023.

Kolditz, O., Fischer, T., Frühwirt, T., Görke, U.-J., Helbig, C., Konietzky, H., Maßmann, J., Nest, M., Pötschke, D., Rink, K., Sattari, A., Schmidt, P., Steeb, H., Wuttke, F., Yoshioka, K., Vowinckel, B., Ziefle, G., and Nagel, T.: GeomInt: geomechanical integrity of host and barrier rocks – experiments, models and analysis of discontinuities, Environ. Earth Sci., 80, 509, https://doi.org/10.1007/s12665-021-09787-0, 2021.

Kolditz, O., Jacques, D., Claret, F., Bertrand, J., Churakov, S. V., Debayle, C., Diaconu, D., Fuzik, K., Garcia, D., Graebling, N., Grambow, B., Holt, E., Idiart, A., Leira, P., Montoya, V., Niederleithinger, E., Olin, M., Pfingsten, W., Prasianakis, N. I., Rink, K., Samper, J., Szöke, I., Szöke, R., Theodon, L., and Wendling, J.: Digitalisation for nuclear waste management: predisposal and disposal, Environ. Earth Sci., 82, 42, https://doi.org/10.1007/s12665-022-10675-4, 2023.

Kolditz, O., McDermott, C., Yoon, J. S., Mollaali, M., Wang, W., Hu, M., Sasaki, T., Rutqvist, J., Birkholzer, J., Park, J.-W., Park, C.-H., Liu, H., Pan, P., Nagel, T., Nguyen, S., Kwon, S., Lee, C., Kim, K.-I., Alexander, B., Hadgu, T., Wang, Y., Zhuang, L., Yoshioka, K., Cunha, G. B., and Fraser-Harris, A.: A systematic model- and experimental approach to hydro-mechanical and thermo-mechanical fracture processes in crystalline rocks, Geomechanics for Energy and the Environment, 41, 100616, https://doi.org/10.1016/j.gete.2024.100616, 2025.

Kühn, M., Tesmer, M., Pilz, P., Meyer, R., Reinicke, K., Förster, A., Kolditz, O., and Schäfer, D.: CLEAN: Project overview on CO_2 large-scale enhanced gas recovery in the Altmark natural gas field (Germany), Environ. Earth Sci., 67, 311–321, https://doi.org/10.1007/s12665-012-1714-z, 2012.

Kurgyis, K., Achtziger-Zupančič, P., Bjorge, M., Boxberg, M. S., Broggi, M., Buchwald, J., Ernst, O. G., Flügge, J., Ganopolski, A., Graf, T., Kortenbruck, P., Kowalski, J., Kreye, P., Kukla, P., Mayr, S., Miro, S., Nagel, T., Nowak, W., Oladyshkin, S., Renz, A., Rienäcker-Burschil, J., Röhlig, K.-J., Sträter, O., Thiedau, J., Wagner, F., Wellmann, F., Wengler, M., Wolf, J., and Rühaak, W.: Uncertainties and robustness with regard to the safety of a repository for high-level radioactive waste: introduction of a research initiative, Environ. Earth Sci., 83, 82, https://doi.org/10.1007/s12665-023-11346-8, 2024.

Lehmann, C., Bilke, L., Buchwald, J., Graebling, N., Grunwald, N., Heinze, J., Meisel, T., Lu, R., Naumov, D., Rink, K., özgür Sen, O., Selzer, P., Shao, H., Wang, W., Zill, F., Nagel, T., and Kolditz, O.: OpenWorkFlow - Development of an open-source synthesis-platform for safety investigations in the site selection process; [OpenWorkFlow - Entwicklung einer Open-Source-Synthese-Plattform für Sicherheitsuntersuchungen im Standortauswahlverfahren], Grundwasser, 29, 31–47, https://doi.org/10.1007/s00767-024-00566-9, 2024.

McDermott, C., Fraser-Harris, A., Sauter, M., Couples, G., Edlmann, K., Kolditz, O., Lightbody, A., Somerville, J., and Wang, W.: New Experimental Equipment Recreating Geo-Reservoir Conditions in Large, Fractured, Porous Samples to Investigate Coupled Thermal, Hydraulic and Polyaxial Stress Processes, Sci. Rep., 8, 14549, https://doi.org/10.1038/s41598-018-32753-z, 2018.

Mollaali, M., Kolditz, O., Hu, M., Park, C.-H., Park, J.-W., McDermott, C. I., Chittenden, N., Bond, A., Yoon, J. S., Zhou, J., Pan, P.-Z., Liu, H., Hou, W., Lei, H., Zhang, L., Nagel, T., Barsch, M., Wang, W., Nguyen, S., Kwon, S., Lee, C., and Yoshioka, K.: Comparative verification of hydro-mechanical fracture behavior: Task G of international research project DECOVALEX–2023, Int. J. Rock Mech. Min., 170, 105530, https://doi.org/10.1016/j.ijrmms.2023.105530, 2023.

Prasianakis, N. I., Haller, R., Mahrous, M., Poonoosamy, J., Pfingsten, W., and Churakov, S. V.: Neural network based process coupling and parameter upscaling in reactive transport simulations, Geochim. Cosmochim. Ac., 291, 126–143, https://doi.org/10.1016/j.gca.2020.07.019, 2020.

Rutqvist, J., Chijimatsu, M., Jing, L., Millard, A., Nguyen, T., Rejeb, A., Sugita, Y., and Tsang, C.: A numerical study of THM effects on the near-field safety of a hypothetical nuclear waste repository – BMT1 of the DECOVALEX III project. Part 3: Effects of THM coupling in sparsely fractured rocks, Int. J. Rock Mech. Min., 42, 745–755, https://doi.org/10.1016/j.ijrmms.2005.03.012, 2005.

Schmidt, P., Steeb, H., and Renner, J.: Investigations into the opening of fractures during hydraulic testing using a hybrid-dimensional flow formulation, Environ. Earth Sci., 80, 497, https://doi.org/10.1007/s12665-021-09767-4, 2021.

Schmidt, P., Steeb, H., and Renner, J.: Diagnosing Hydro-Mechanical Effects in Subsurface Fluid Flow Through Fractures, Pure Appl. Geophys., 180, 2841–2860, https://doi.org/10.1007/s00024-023-03304-z, 2023.

Sjöberg, L.: Local acceptance of a high-level nuclear waste repository, Risk Anal., 24, 737–749, https://doi.org/10.1111/j.0272-4332.2004.00472.x, 2004.

Sjöberg, L. and Drottz-Sjöberg, B.-M.: Risk perception by politicians and the public, Energy and Environment, 19, 455–483, https://doi.org/10.1260/095830508784641408, 2008.

Sneddon, I. and Lowengrub, M.: Crack problems in the classical theory of elasticity, The SIAM series in Applied Mathematics, John Wiley & Sons, ISBN 0471808458, 9780471808459, 1969.

Sun, C., Zhuang, L., Jung, S., Lee, J., and Yoon, J. S.: Thermally induced slip of a single sawcut granite fracture under biaxial loading, Geomechanics and Geophysics for Geo-Energy and Geo-Resources, 7, 96, https://doi.org/10.1007/s40948-021-00293-y, 2021.

Sun, C., Zhuang, L., Yoon, J. S., and Min, K.-B.: Thermally induced shear reactivation of critically-stressed smooth and rough granite fractures, IOP Conference Series: Earth and Environmental Science, 1124, 012119, https://doi.org/10.1088/1755-1315/1124/1/012119, 2023.

Sun, C., Zhuang, L., Youn, D. J., Yoon, J. S., and Min, K.-B.: Laboratory investigation of thermal stresses in fractured granite: Effects of fracture surface roughness and initial stress, Tunn. Undergr. Sp. Tech., 145, 105610, https://doi.org/10.1016/j.tust.2024.105610, 2024.

Sun, C., Zhuang, L., Yoon, J., and Min, K.: Experimental insights into frictional resistance and slip pattern of granite fractures and implications for thermoshearing prediction, Earth Energy Sci., accepted, 2025.

The University of Edinburgh (UK) and Chongqing University (China): DECOVALEX [data set], http://www.decovalex.org, last access: 17 March 2025.

Yi, H., Zhou, H., Kolditz, O., and Xue, D.: Insight into the elasto-plastic behavior of Beishan granite influenced by temperature and hydraulic pressure, Int. J. Rock Mech. Min., 177, 105744, https://doi.org/10.1016/j.ijrmms.2024.105744, 2024.